



## Quasi-static and dynamic analyses of thin-webbed high-speed gears: Centrifugal effect influence

Bérengère Guilbert, Philippe Velex, Philippe Cutuli

### ► To cite this version:

Bérengère Guilbert, Philippe Velex, Philippe Cutuli. Quasi-static and dynamic analyses of thin-webbed high-speed gears: Centrifugal effect influence. Proceedings of the Institution of Mechanical Engineers, Part C: Journal of Mechanical Engineering Science, 2019, 233 (21-22), pp.095440621985541. 10.1177/0954406219855411 . hal-02162278

HAL Id: hal-02162278

<https://hal.science/hal-02162278>

Submitted on 9 Apr 2024

**HAL** is a multi-disciplinary open access archive for the deposit and dissemination of scientific research documents, whether they are published or not. The documents may come from teaching and research institutions in France or abroad, or from public or private research centers.

L'archive ouverte pluridisciplinaire **HAL**, est destinée au dépôt et à la diffusion de documents scientifiques de niveau recherche, publiés ou non, émanant des établissements d'enseignement et de recherche français ou étrangers, des laboratoires publics ou privés.

# Quasi-static and dynamic analyses of thin-webbed high-speed gears: Centrifugal effect influence

B Guilbert<sup>1,2</sup>, P Velex<sup>2</sup> and P Cutuli<sup>1</sup>

## Abstract

The objective of this paper is to analyse the effect of centrifugal effects on thin-rimmed/-webbed gears. To this end, an original hybrid gear model is used, which combines lumped parameter elements, finite elements and condensed sub-structures along with a mortar-based mesh interface aiming at coupling mismatched models. It is shown that due to gear body flexibility, centrifugal effects can strongly modify geometry and, consequently, tooth load distributions at high speeds. The possibility to counterbalance these effects by introducing profile and lead modification is investigated. It is finally shown that for the effective tooth design, both thin-rimmed gear geometry and operating conditions must be accounted for.

## Keywords

High-speed gears, centrifugal effects, hybrid models, lead crown, profile modifications

## Introduction

Gear dynamics has been studied extensively and a large number of models can be found in the literature,<sup>1–6</sup> which generally rely on the hypothesis of rigid body gears connected by an elastic mesh interface, often reduced to a time-varying, possibly non-linear, scalar stiffness function. In the case of helicopter transmissions, however, thin-rimmed high-speed gears are employed, which can hardly be simulated using lumped parameter elements and require more advanced modelling strategies. In this context, Parker et al.<sup>7</sup> developed a bi-dimensional spur gear model combining finite elements and an analytical contact model, while Kahraman et al.<sup>8</sup> introduced a full three-dimensional (3D) finite element (FE) model to represent the actual gear geometry. In order to limit the computational times due to large FE models, Abousleiman et al.<sup>9,10</sup> and Bettaieb et al.<sup>11</sup> proposed a model reduction technique based on a Ritz method using truncated sets of mode shapes<sup>12</sup> making it possible to simultaneously account for the system dynamic behaviour and the instant contact conditions on tooth flanks. In the same vein, Eritenel and Parker<sup>13</sup> introduced a full contact model as well as bulk stiffness for rim deflections and simulated partial and total contact losses at high speeds. Shweiki et al.<sup>14</sup> simulated various lightweight designs and showed that thin and hollow webs were influential on jump and contact loss phenomena. The effect

of rotational speed has been studied on the modal and dynamic behaviour of discs,<sup>15–17</sup> disk-spindle systems<sup>18,19</sup> and thick cylindrical shells.<sup>20</sup> However, the studies on the specific role of speed on gear dynamics including centrifugal effects remain sparse. Gyroscopic effects have been considered in planetary gears models either based on lumped parameters<sup>21–23</sup> or with deformable ring gears<sup>24</sup> to analyse the influence of speed on dynamic tooth loads and ring-gear modal response. Finally, Li<sup>25–28</sup> used 3D static FE models incorporating centrifugal effects as additional forcing terms to analyse rim deflections, root stresses and tooth load distributions in thin-webbed gears.

The main objective of this paper is therefore to extend the analysis of centrifugal effects to the dynamic behaviour of thin-rimmed/-webbed gears. To this end, a 3D FE model of lightweight gears is condensed and introduced in a hybrid dynamic model combining lumped parameters and deformable sub-structures in which the contributions of centrifugal effects are embedded.

<sup>1</sup>Turbomeca, R&T Department, Bordes, France

<sup>2</sup>INSA Lyon, Université Lyon, LaMCoS, France

### Corresponding author:

P Velex, INSA Lyon, Université Lyon, 20 Avenue Albert Einstein, UMR CNRS 5259, Villeurbanne 69621, France.  
Email: philippe.velex@insa-lyon.fr

## Dynamic hybrid models – basic principles

For the sake of conciseness, only the main modelling principles are presented in this section while the complete technical details can be found in Guilbert et al.<sup>29</sup> The hybrid model in Figure 1 combines lumped parameters and 3D finite elements. The pinion and mesh interface are simulated using the method of Velex and Maatar,<sup>3</sup> whereas the deformable gear body is accounted for by a substructure<sup>30</sup> derived from a full 3D finite element model with brick elements condensed at its rim and bearing nodes. In this paper, the housing and bearings are simulated as additional stiffness elements. A time-varying, non-linear Winkler foundation model is used to simulate mesh elasticity and tooth flank deviations, which connects the six degrees of freedom (DOFs) at the pinion centre (three translations and three rotations) to the DOFs (three translations per node only) at the rim contour nodes of the sub-structured gear body. The normal deflection at any potential point of contact  $M_{ij}$  reads

$$\Delta(M_{ij}) = \mathbf{V}(M_{ij})^T \mathbf{X} - \delta_0(M_{ij}) \quad (1)$$

where  $\mathbf{V}(M_{ij})^T = [\mathbf{n}_1 \ \mathbf{n}_1 \times \mathbf{M}_{ij}\mathbf{O}_1 \ \mathbf{n}_2]$ , structural vector;  $M_{ij}$  is the contact point of the  $j$ th segment of the  $i$ th line of contact;  $\mathbf{n}_2 = -\mathbf{n}_1$  with  $\mathbf{n}_1$  being the unit outward normal vector with respect to the pinion tooth flanks; and  $\mathbf{X} = \{\mathbf{u}_1(O_1) \ \omega_1 \ \mathbf{u}_2(M_{ij})\}^T$ , DOF vector expressed at the pinion centre  $O_1$  and the tooth root  $M_{p_{ij}}$  of the gear.

The direct collocation of the discrete foundation stiffness elements with the gear continuous FE models would induce numerical spikes on tooth load distributions since the two models are not compatible.<sup>31</sup> In order to avoid such numerical flaws, a mortar-based interface has been added to smoothen the transition between the discretised contact lines and the sub-structure degrees of freedom. Details about the theory and implementation can be found in literature.<sup>29,31</sup> The corresponding modified equations are

$$\Delta(M_{ij}) = \mathbf{V}^*(M_{ij})^T \mathbf{X}_m - \delta_0(M_{ij}) \quad (2)$$

where  $\mathbf{V}^*(M_{ij})^T$  is the modified structural vector at contact point  $M_{ij}$

$$\mathbf{V}^*(M_{ij})^T = \left[ \begin{array}{l} \left\{ \mathbf{n}_1^T (\mathbf{n}_1 \times \mathbf{M}_{ij}\mathbf{O}_1)^T \right\} \\ \left\{ \left( \frac{1}{2} \mathbf{n}_2^T + \lambda_p(M_{ij}) \kappa_p \right) \mathbf{I}_{int}^T \right\} \\ \left\{ \times \left( \frac{1}{2} \mathbf{n}_2^T - \lambda_p(M_{ij}) \kappa_p \right) \mathbf{I}_{int}^T \right\} \end{array} \right]$$

$\mathbf{X}_m = \{\mathbf{u}_1(O_1) \ \omega_1 \ \mathbf{X}_2\}$  new DOF vector,  $\mathbf{X}_2$  is the DOF vector associated with the sub-structure,

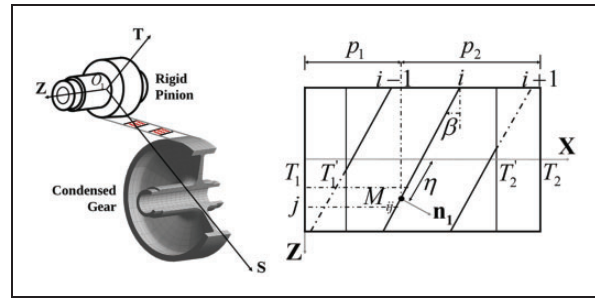


**Figure 1.** Hybrid model and base plane parameters (only a fraction of the gear is represented).

$\lambda_p(M_{ij})$ ,  $\kappa_p$  and  $\mathbf{I}_{int}$  are the specific additional terms brought by the mortar interface.<sup>29,31</sup>

The mesh stiffness matrix and load vector are finally derived as

$$\begin{aligned} [K_{12}(t)] &= \sum_i \sum_j k_{ij} \mathbf{V}^*(M_{ij}) \mathbf{V}^*(M_{ij})^T \\ F_{12}(t) &= \sum_i \sum_j k_{ij} \delta_0(t) \mathbf{V}^*(M_{ij}) \end{aligned} \quad (3)$$

The global model is obtained by assembling all the component models (shaft, rigid pinion, bearing/casing stiffness elements) along with the gear substructure and the mesh Winkler foundations. Following Guilbert et al.,<sup>29</sup> the centrifugal load vector is extracted from the FE model leading to the following equations of motion

$$[\mathbf{M}] \ddot{\mathbf{X}} + [\mathbf{C}] \dot{\mathbf{X}} + [\mathbf{K}(t)] \mathbf{X} = [\mathbf{F}(t) + \mathbf{F}_c] \quad (4)$$

with  $\mathbf{F}_c$  being the centrifugal load vector for the condensed part of the system.

The resulting differential system is solved by combining a Newmark time-step integration scheme with the normal contact algorithm in Velex and Maatar<sup>3</sup> making it possible to simulate the total and partial contact losses between the teeth.

Finally, the proposed hybrid model can easily be extended to account for a deformable pinion whose substructure contour nodes are connected to the contact line discrete model by using the same two-point connection and mortar-based interface,<sup>29,31</sup> thus leading to a fully flexible pinion and gear model. Such hybrid models have been validated by comparing the simulation results with experimental evidence and numerical findings from full quasi-static FE model,<sup>29</sup> which comprises quasi-static contact pressure distributions, gear body modal behaviour and dynamic rim displacements.

## Solid pinion and thin-webbed gear

### Influence of centrifugal effects

The gear geometry under consideration is defined in Table 1 and corresponds to a helicopter power

transmission with helical gears of relatively large rim ( $b=40$  mm).

The pinion shaft geometry in Figure 2(a) is relatively compact so that a rigid disc and beam elements can be used. On the other hand, the thin-webbed gear (Figure 2(b)) is modelled by three-dimensional finite elements condensed at the contour nodes distributed on the rim outer face and at the bearing centres where casing/bearing stiffness elements are attached.

Considering first quasi-static conditions i.e. the dynamic model at very low speed ( $\Omega_S = 0.1$  r/min (0.01 rad/s)), the results in Figure 3 show that the pressure distribution on tooth flanks is centred and symmetric, thus illustrating the capacity for flexible thin webs to compensate for the misalignments possibly induced by the axial component of the mesh force caused by helical gears.

Simulations are extended over the full speed range (0–28,650 r/min (3000 rad/s)) and the resulting dynamic tooth load factor (maximum dynamic-to-static mesh force ratio) versus speed is plotted in Figure 4. The configurations with and without centrifugal effects have been tested and it can be observed that, as expected, tooth loading is modified mainly in the high-speed range.

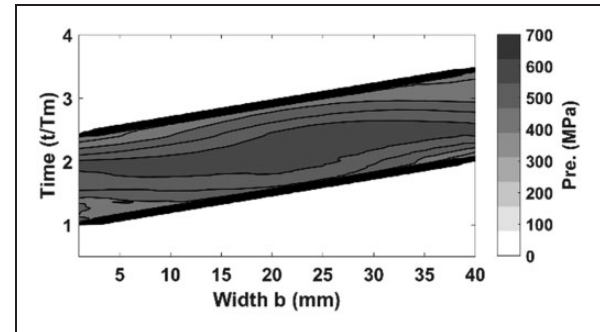
**Table 1.** Helical gear geometry.

	Pinion	Gear
Module $m$ (mm)	2.5	2.5
Number of teeth	35	68
Pressure angle (°)	25	25
Helix angle (°)	12	12
Addendum coefficient	0.976	0.970
Dedendum coefficient	1.262	1.268
Profile shift coefficient	0.275	0.317
Fillet radius/module	0.25	0.25
Rim width $b$ (mm)	40	40

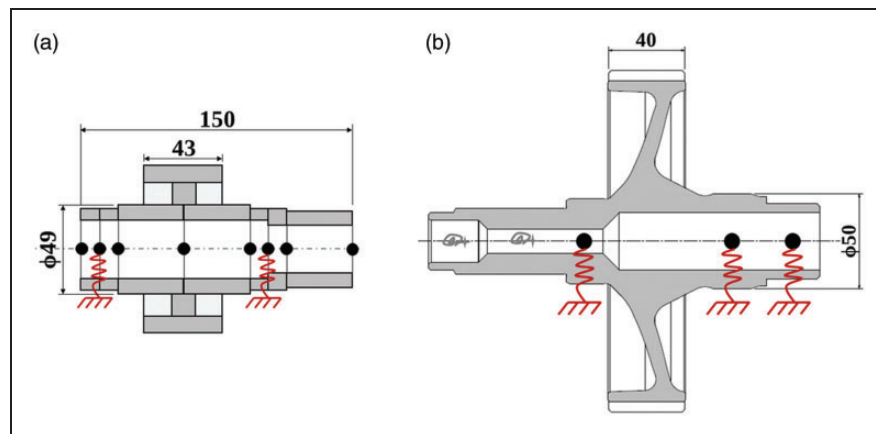
This influence is investigated further by considering the dynamic pressure patterns on tooth flanks at three different speeds which correspond to: (i) the quasi-static conditions and, (ii) two non-resonant speeds of 14,325 r/min (1500 rad/s) (slight influence of centrifugal effects) and 28,650 r/min (3000 rad/s) (larger influence) on the pinion shaft based on the results in Figure 4.

Figure 5 shows the local pressure distributions on one tooth flank obtained by using the hybrid model when centrifugal effects are discarded (left column) and included (right column). It is found that the pressure distributions in the absence of centrifugal effects (left graphs) are independent of speed with the highest pressure located above the rim-web connection, which corresponds to the most rigid part of the tooth contact. However, speed becomes influential when considering centrifugal forces and leads to increasingly asymmetric patterns across the face-width as speed increases. For the highest speed  $\Omega_2 = 28,650$  r/min (3000 rad/s), pressure peaks near the tooth edge are observed which can cause severe contact failures.

The root cause of this phenomenon is the deformed shape of the thin-web/rimmed gear as illustrated in Figure 6. The deflection of the cantilever part of the



**Figure 3.** Quasi-static pressure distribution.



**Figure 2.** (a) Pinion geometry with beam model; (b) thin-webbed gear definition, modelled with condensed FE – springs represent casing/bearings, torsional springs represent splines (resisting torque).

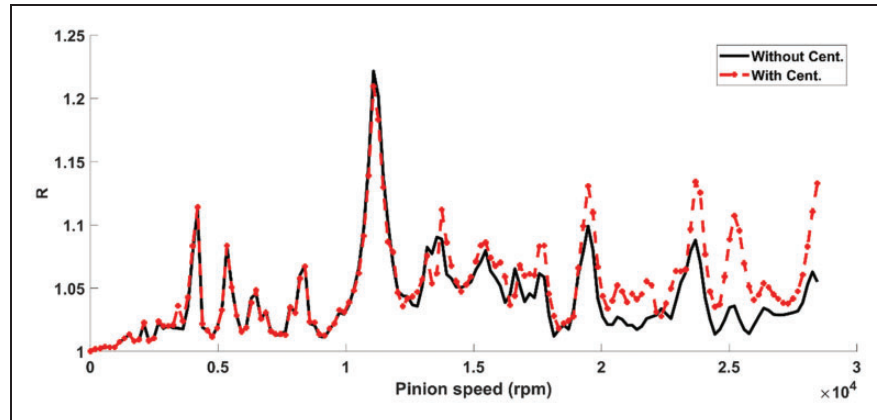


**Figure 4.** Dynamic tooth load factor with and without centrifugal effects (thin-rimmed gear).

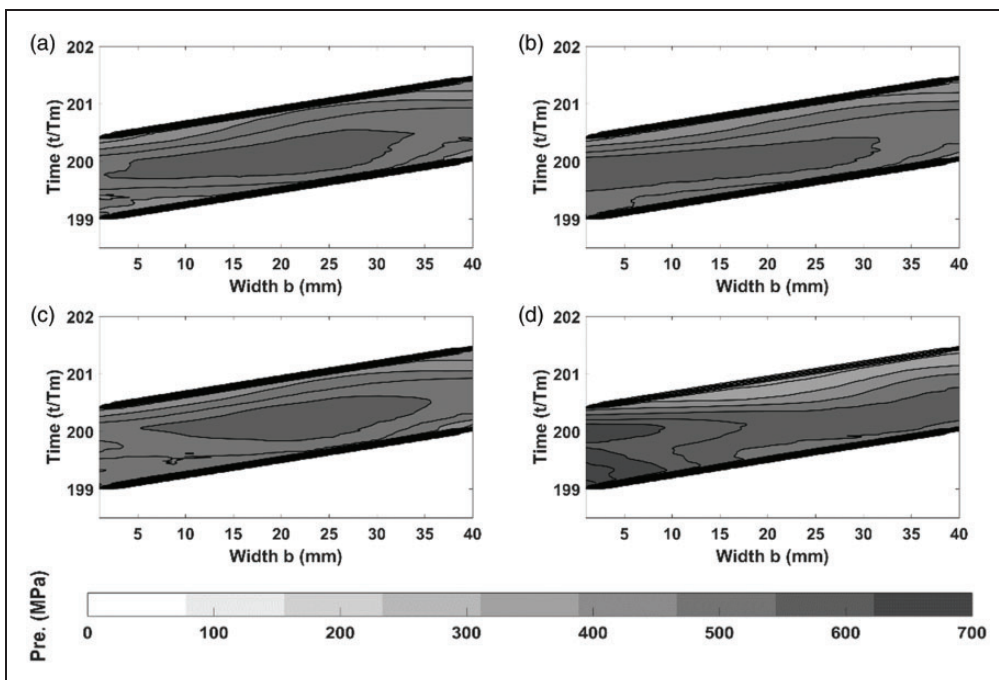


**Figure 5.** Centrifugal effect influence on pressure distribution: (a)  $\Omega_1$ , without centrifugal effects; (b)  $\Omega_1$ , with centrifugal effects; (c)  $\Omega_2$ , without centrifugal effects; (d)  $\Omega_2$ , with centrifugal effects.

gear rim at the maximum speed is non-uniform in the face-width direction with a maximum amplitude of 85  $\mu\text{m}$ , significantly larger than the mesh deflection at one extremity. In these conditions, the tooth flanks are skewed and the tooth edges with maximum deflection are overloaded. Despite significant modifications in gear shape, it was observed that the influence on the actual mesh geometrical characteristics remains negligible since, for the largest centrifugal deflections, the base radius is increased by 0.1%, leading to a 0.5% variation in pressure angle.

#### Optimisation – influence of crowning

In view of the deformed shape in Figure 6, lead parabolic crown (Figure 7) of amplitude  $A$  ranging from 5 to 20  $\mu\text{m}$  are introduced. The results in Figure 8(a)

show the corresponding maximum pressure over one mesh period at  $\Omega_1 = 14,325 \text{ r/min}$  (1500 rad/s) for various amplitudes  $A$ . In this case, a light crown (5–10  $\mu\text{m}$ ) seems sufficient to eliminate the overloads at both rim ends and larger modifications would only increase the maximum pressure and, consequently, be detrimental. Figure 8(b) shows the complete pressure distribution obtained with a 5  $\mu\text{m}$  crowning, which confirms that the load pattern is well-centred and that the maximum pressure is only marginally higher than that obtained for quasi-static conditions without any modification.

The same study is conducted at the maximum speed of 28,650  $\text{r/min}$  (3000 rad/s) (Figure 9(a)). In this case, a 5  $\mu\text{m}$  crowning is not sufficient to re-establish a uniform load and amplitudes in the range 10–15  $\mu\text{m}$  are preferable, whereas a 20  $\mu\text{m}$  crown is

not appropriate as it unloads one tooth edge. These findings are confirmed by the tooth load pressure distribution in Figure 9(b).

The improvement brought by crowning on load distributions is confirmed when analysing the dynamic mesh forces at 14,325 r/min (1500 rad/s) and 28,650 r/min (3000 rad/s) represented by the

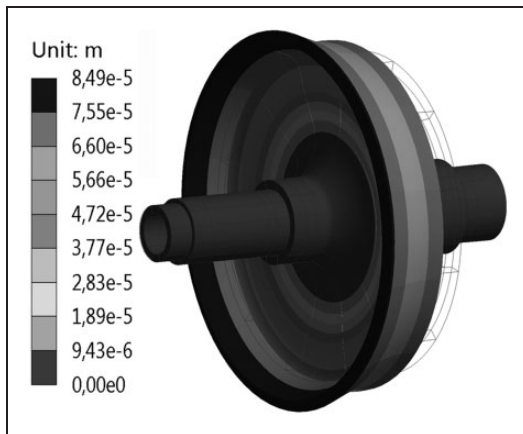


**Figure 6.** Gear deflection under centrifugal effects (at 28,650 r/min (3000 rad/s)) for the whole gear.

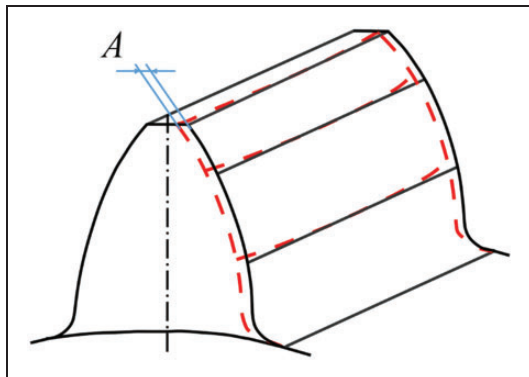


**Figure 7.** Crown definition ( $A$  is the crown amplitude).

maximum dynamic-to-static mesh force ratios in Figure 10. Figure 10(a) ( $\Omega_1 = 14,325$  r/min) shows that dynamic mesh forces are moderate and almost insensitive to crowning. The situation is different at the maximum speed  $\Omega_2$  for which centrifugal effects are significant and a clear optimum is observed for a 10- $\mu\text{m}$  crown. Smaller or larger amplitudes induce more dynamic force amplifications suggesting that a 10- $\mu\text{m}$  amplitude is the best compromise over the whole speed range.

#### Profile modification – optimisation with regard to transmission error

In addition to lead modifications, profile modifications are frequently employed to reduce gear noise and vibrations. In what follows, symmetric linear tip relief is considered (same on the pinion and gear tooth tips) and optimisation is conducted based on the time-variations of quasi-static transmission error under load. Systematic sweeps have been performed over the modification depth at tooth tips  $E$  (in  $\mu\text{m}$ ) and dimensionless extents of modification  $\Gamma$  in the profile direction leading to the level curves in Figures 11 and 12 for the example treated. When centrifugal effects are ignored, it can be noticed in Figure 11(a) that the optimum set of relief agrees well with the analytical so-called Master Curves where transmission error is found to be optimum in the case of solid gears with symmetric linear relief of depth  $E$  and normalised extents of modification  $\Gamma$ .<sup>32</sup> The introduction of the maximum centrifugal effects at  $\Omega_2 = 28,650$  r/min (3000 rad/s) (Figure 11(b)) dramatically modifies the best profile modification area, which no longer matches with the analytical Master Curve. Larger tip relief amplitudes are required because of the additional gear deflections and the uneven tooth load distributions in the face-width direction caused by centrifugal forces (see Figure 5(d)).

If lead crown is superimposed (Figure 12), transmission error is not improved in spite of a better load

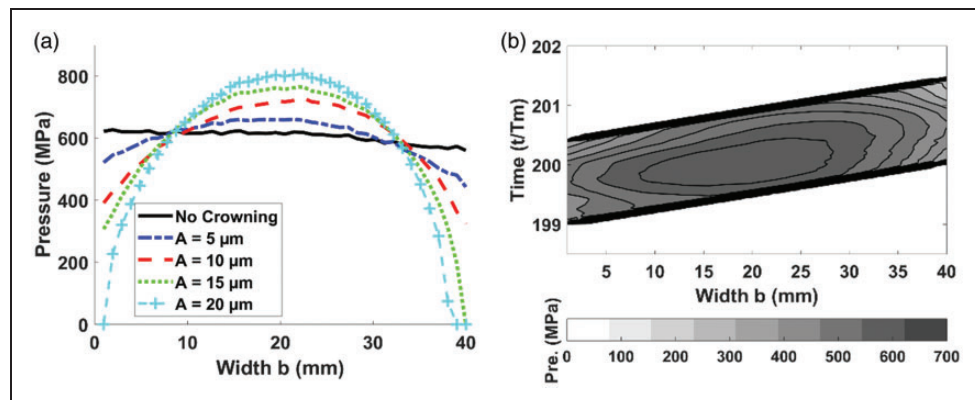


**Figure 8.** Crowning effect on pressure distribution at middle-range speed (14,325 r/min (1500 rad/s)): (b)  $A = 5 \mu\text{m}$ .

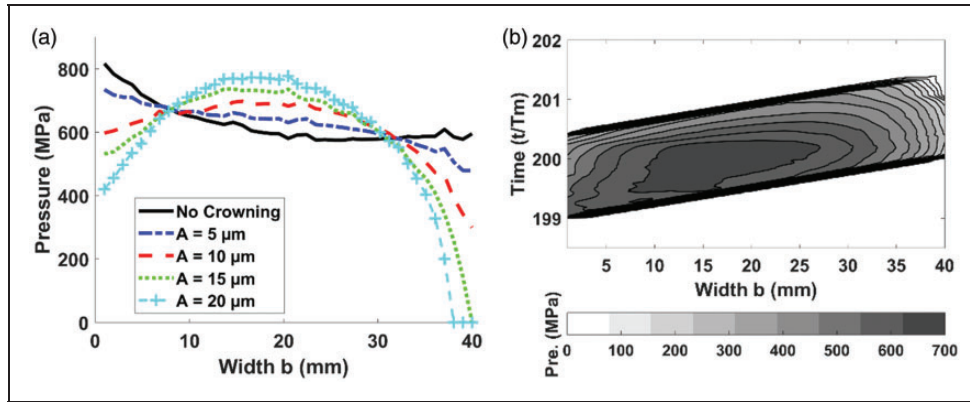


**Figure 9.** Crowning effect on pressure distribution at high speed (28,650 r/min (3000 rad/s)): (b)  $A = 10 \mu\text{m}$ .

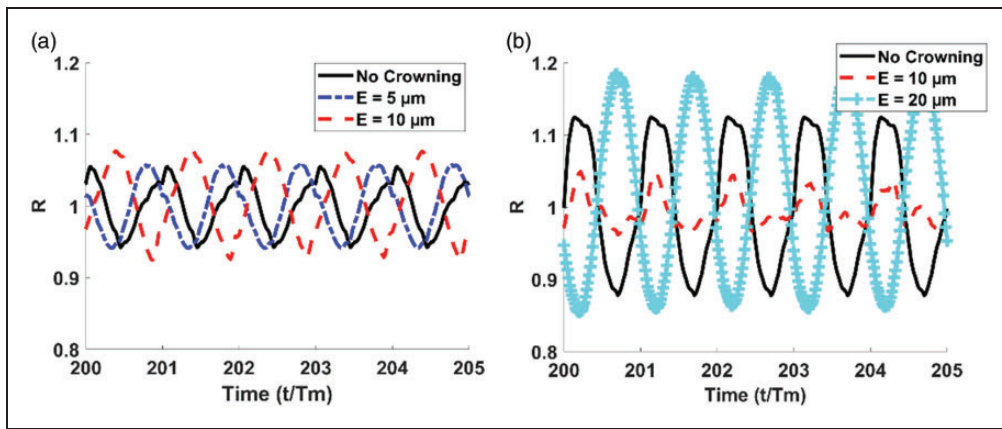


**Figure 10.** Associate dynamic ratio for each crowning at both speed: (a)  $\Omega_1$ ; (b)  $\Omega_2$ .

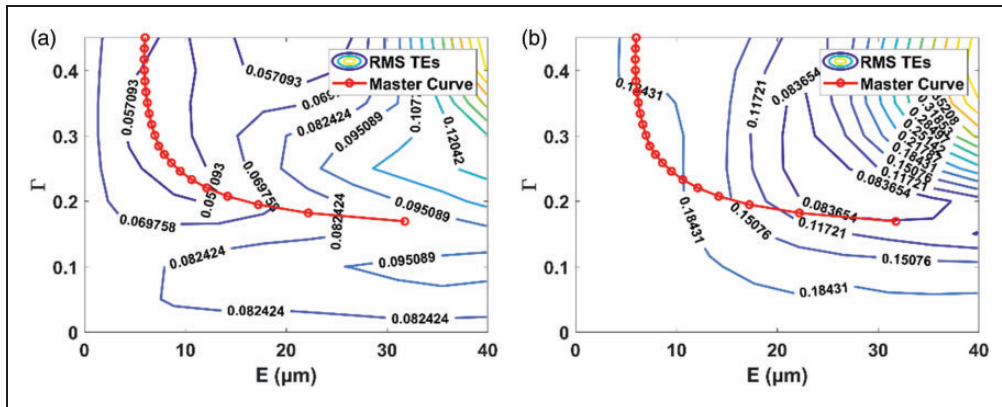


**Figure 11.** Optimisation with regard to the TEs for: (a) centrifugal effects at zero speed and (b) centrifugal load for  $\Omega_2 = 28,650 \text{ r/min}$  (3000 rad/s).

distribution. The overall root mean square of transmission error is higher and the optimum reliefs with respect to transmission error are still far from what was found in the absence of centrifugal effects. It can be observed that long profile reliefs appear as more sensitive to variations in profile amplitude, whereas short reliefs are more tolerant and would therefore

be an interesting choice for systems with several different operating conditions.

### Thin-webbed pinion and gear

The thin-webbed pinion in Figure 13 with the same tooth geometry as above is now considered and

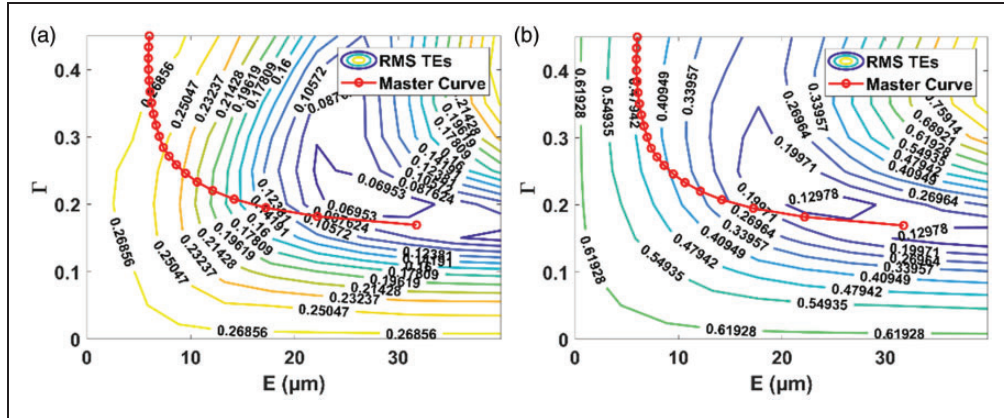


**Figure 12.** Effect of crowning on profile modification optimum (with centrifugal effects at  $\Omega_2$ ): (a)  $A = 10 \mu\text{m}$ ; (b)  $A = 20 \mu\text{m}$ . RMS TEs: root mean square transmission errors.

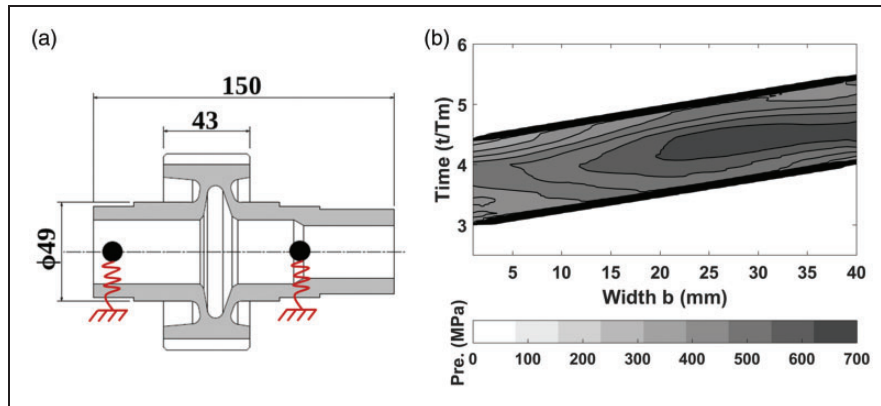


**Figure 13.** (a) New pinion geometry and (b) associated quasi-static pressure distribution.

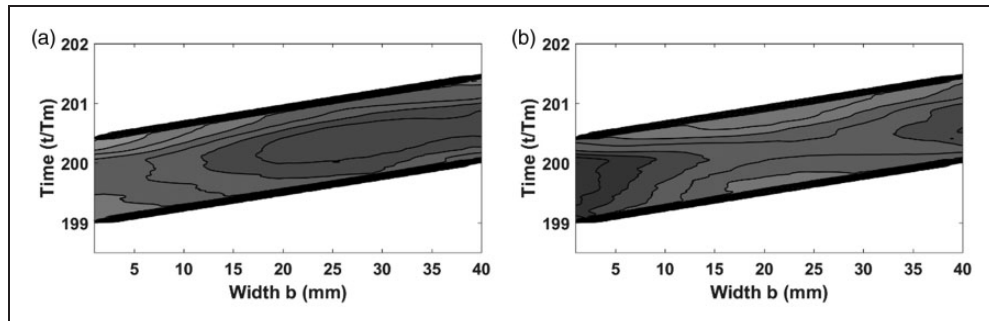


**Figure 14.** Centrifugal effect influence on pressure distribution for fully webbed gear: (a)  $\Omega_2$ , without centrifugal effects; (b)  $\Omega_2$ , with centrifugal effects.

a second sub-structure is introduced in the place of the rigid disc + shaft element model used in the previous section.

Figure 13(b) shows the quasi-static pressure distribution with both condensed pinion and gear. Compared with the previous findings for a rigid pinion (Figure 3), it can be noticed that the maximum pressure zone has moved to a location corresponding to the rim-web connections on the pinion and gear (Figure 13(a) and Figure 2(b)).

The dynamic tooth load factor over the whole speed is very similar to what is found in Figure 4, thus showing no obvious contribution of the thin-webbed pinion at such. Focusing on tooth load distributions at high speeds for which centrifugal effects are prominent, Figure 14(b) shows that that thin-webbed pinion and gear lead to overloads at both edges of the tooth flanks in contrast with the one-sided loading found with a thin-webbed gear only.

Here too, the physical reason is the asymmetric deformed shapes of both the pinion and gear across the face width generated by centrifugal forces (Figures 6 and 15).

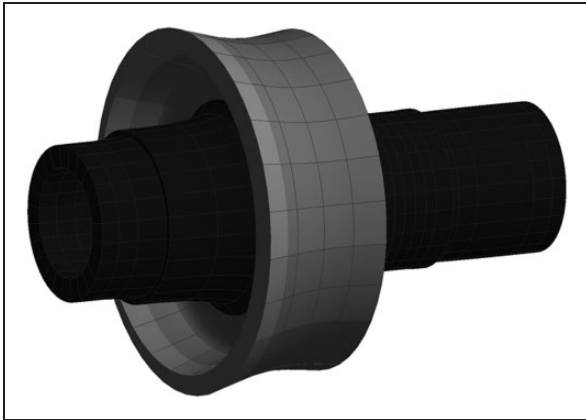


**Figure 15.** Pinion deflection under centrifugal effects.

In view of the tooth load distribution on tooth flanks, lead crown appears as an interesting solution and the results in Figure 16 prove that a 10 µm crown amplitude can effectively improve the contact conditions on tooth flanks by centring the pressure pattern.

Turning to transmission error time-variations, systematic sweeps over the profile relief parameters (depth and extent) are performed leading to the following conclusions:

- (a) With or without centrifugal effects, the reliefs minimizing transmission error time-variations for both a pinion and gear with thin webs are closer to the analytical Master Curve for solid gears (Figure 17) than in the case of a thin-webbed gear only,
- (b) The superposition of a 10 µm lead crown (Figure 18) does not alter the previous results significantly, suggesting that, as long as the tooth load distribution across the face width remains symmetrical, the profile reliefs minimizing transmission error variations are close to those found for solid gears.

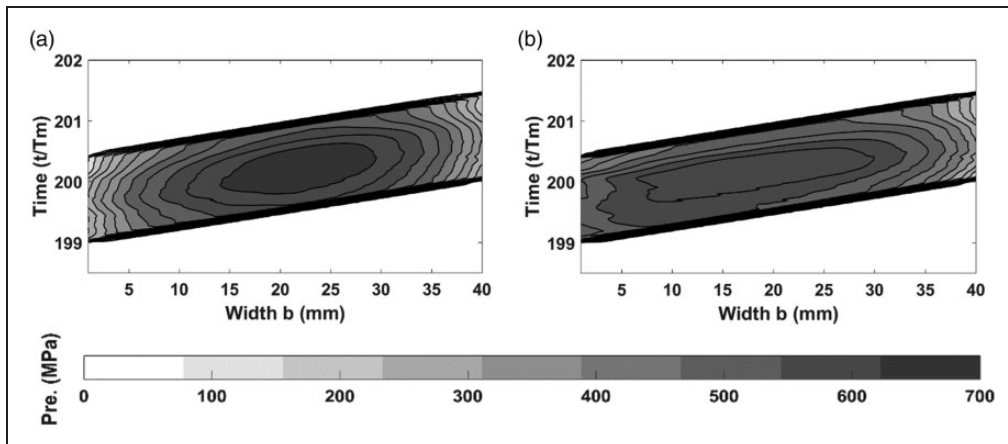


**Figure 16.** 10 µm crowning for both studied speed with both flexible pinion and wheel. (a)  $\Omega_1$  and (b)  $\Omega_2$ .

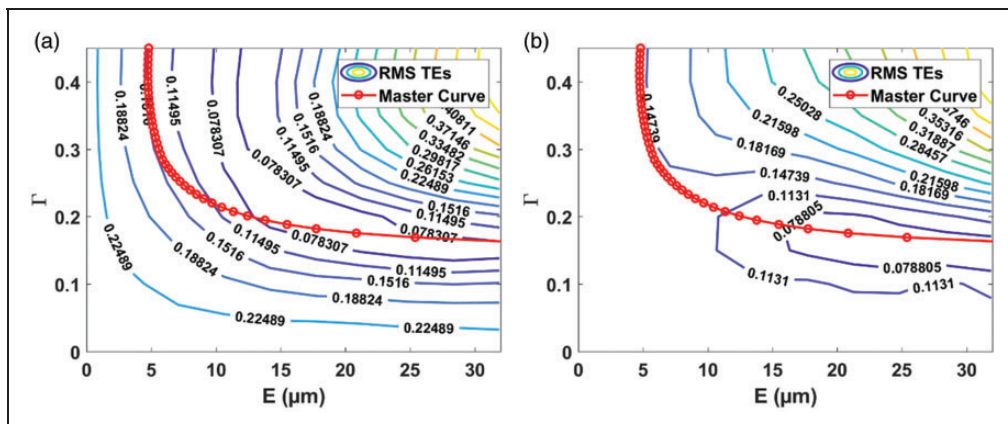


**Figure 17.** Optimisation with regard to the TEs for: (a) centrifugal effects at zero speed and (b) centrifugal load for  $\Omega_2 = 28,650$  r/min (3000 rad/s).

RMS TEs: root mean square transmission errors.

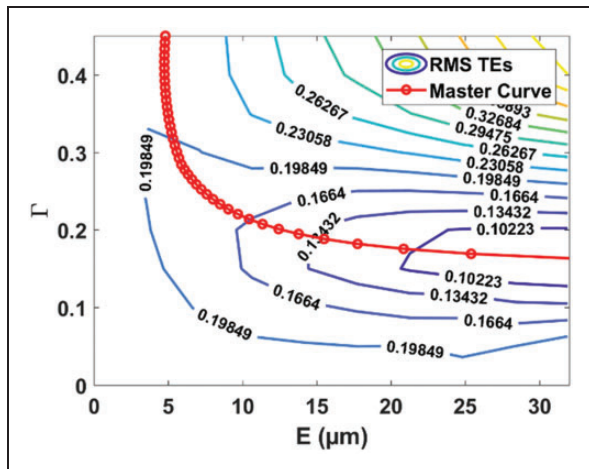


**Figure 18.** Effect of 10  $\mu\text{m}$  crowning on profile modification optimum (with centrifugal effects at  $\Omega_2 = 28,650 \text{ r/min}$  (3000 rad/s)).

RMS TEs: root mean square transmission errors.

## Conclusions

Hybrid modular models have been presented which are able to capture the dynamic contact conditions in thin-rimmed-/webbed gears and particularly the influence of centrifugal effects at high speeds. It has been shown that centrifugal effects in thin-webbed pinions and/or gears at high speeds can alter tooth contact conditions significantly and that specific models are therefore needed in order to define the most interesting profile and lead modifications. Lead crown can improve the contact conditions at very high speed to a large extent, whereas contrasted trends are reported concerning the combination of profile relief and lead crown minimizing transmission error. It is noticed that although tooth load distributions are improved, the introduction of lead crowning usually deteriorates transmission error. The symmetry of the tooth load distribution across the face width appears as an influential parameter on the definition of optimum profile modifications. As long as load symmetry is conserved, the profile reliefs minimizing transmission error are close to those defined in the case of solid gears, whereas when it is no longer the case e.g. one tooth edge is overloaded for instance, the optimum relief parameters strongly deviate from those obtained for solid gears.

From a practical viewpoint, it can be concluded that advanced models incorporating pinion/gear body deflections are certainly needed to calculate tooth load distributions on thin-webbed high-speed gears since the combined influence of web geometry and centrifugal forces can be crucial on tooth contacts. However, dynamic tooth load factors seem far less sensitive to pinion/gear body elasticity and centrifugal effects, suggesting that less refined dynamic models can be sufficient to calculate tooth critical speeds.

## Declaration of Conflicting Interests

The author(s) declared no potential conflicts of interest with respect to the research, authorship, and/or publication of this article.

## Funding

The author(s) disclosed receipt of the following financial support for the research, authorship, and/or publication of this article: The author would like to thank SAFRAN Helicopter Engines and the ANRT (French National Association for Research and Technology), for their support via the CIFRE grant attributed to B. Guilbert. The support of the INSA-SAFRAN Chair on *Innovative Mechanical Transmission for Aeronautics* is gratefully acknowledged.

## ORCID iD

P Velex  <https://orcid.org/0000-0002-5452-2942>

## References

- Özgüven HN and Houser DR. Mathematical models used in gear dynamics – a review. *J Sound Vib* 1988; 121: 383–411.
- Kahraman A and Singh R. Non-linear dynamics of a spur gear pair. *J Sound Vib* 1990; 142: 49–75.
- Velex P and Maatar M. A mathematical model for analysing the influence of shape deviation and mounting errors on gear behaviour. *J Sound Vib* 1996; 191: 629–660.
- Baud S and Velex P. Static and dynamic tooth loading in spur and helical geared systems-experiments and model validation. *ASME J Mech Des* 2002; 124: 334–346.
- Vedmar L and Andersson A. A method to determine dynamic loads on spur gear teeth and on bearings. *J Sound Vib* 2003; 267: 1065–1084.
- Kubur M, Kahraman A, Zini DM, et al. Dynamic analysis of a multi-shaft helical gear transmission by finite elements: model and experiment. *ASME J Vib Acoust* 2004; 126: 398–406.
- Parker RG, Vijayakar SM and Imajo T. Non-linear dynamic response of a spur gear pair: modelling and experimental comparisons. *J Sound Vib* 2000; 237: 435–455.
- Kahraman A, Kharazi AA and Umrani M. A deformable body dynamic analysis of planetary gears with thin rims. *J Sound Vib* 2003; 262: 752–768.
- Abousleiman V and Velex P. A hybrid 3D finite element/lumped parameter model for quasi-static and dynamic analysis of planetary/epicyclic gear sets. *Mech Mach Theory* 2006; 41: 725–748.
- Abousleiman V, Velex P and Becquerell S. Modelling of spur and helical gear planetary drives with flexible gears and planet carriers. *J Mech Des* 2007; 129: 95–106.
- Bettaieb M, Velex P and Ajmi M. A static and dynamic model of geared transmission by combining substructures and elastic foundations – application on thin-rimmed gears. *J Mech Des* 2007; 129: 184–194.
- Abousleiman V. *Comportement dynamique des trains planétaires et épicycloïdaux, conditions de contact instantanées et sous-ensembles flexibles*. PhD Thesis, INSA Lyon, France, 2004.

13. Eritenel T and Parker RG. Three-dimensional non-linear vibration of gear pairs. *J Sound Vib* 2012; 331: 3628–3648.
14. Shweiiji S, Palermo A and Mundo D. A study on the dynamic behaviour of lightweight gears. *Shock Vib* 2017; 7982170.
15. Tobias SA and Arnold RN. The influence of dynamical imperfection on the vibration of rotating disks. *Proc Instn Mech Engrs* 1957; 171: 669–690.
16. Mote CD Jr. Stability of circular plates subjected to moving loads. *J Franklin Inst* 1970; 290: 329–344.
17. Hutton SG, Chonan S and Lehman BF. Dynamic response of a guided circular saw. *J Sound Vib* 1987; 112: 527–539.
18. Parker RG and Sathe PJ. Exact solution for the free and forced vibration of a rotating disk-spindle system. *J Sound Vib* 1999; 223: 445–465.
19. Parker RG and Sathe PJ. Free vibration and stability of a spinning disk-spindle system. *J Vib Acoust* 1999; 121: 391–396.
20. Guo D, Chu FL and Zheng ZC. The influence of rotation on vibration of a thick cylindrical shell. *J Sound Vib* 2001; 242: 487–505.
21. Eritenel T and Parker RG. Modal properties of a three-dimensional helical planetary gears. *J Sound Vib* 2009; 325: 397–420.
22. Cooley CG and Parker RG. Vibration properties of high-speed planetary gears with gyroscopic effects. *ASME J Vib Acoust* 2012; 134: 061014–061014-11.
23. Cooley CG and Parker RG. Unusual gyroscopic system eigenvalue behaviour in high-speed planetary gears. *J Sound Vib* 2013; 332: 1820–1828.
24. Cooley CG and Parker RG. Vibration of high-speed rotating rings coupled to space-fixed stiffnesses. *J Sound Vib* 2014; 333: 2631–2648.
25. Li S. Deformation and bending stress analysis of a three-dimensional thin-rimmed gear. *J Mech Des* 2002; 124: 129–135.
26. Li S. Contact stress and root stress analyses of thin-rimmed spur gears with inclined webs. *J Mech Des* 2012; 134: 051001–1–051001-13.
27. Li S. Centrifugal load and its effects on bending strength and contact strength of high speed thin-walled spur gear with offset web. *Mech Mach Theory* 2008; 43: 217–239.
28. Li S. Effect of centrifugal load on tooth contact stresses and bending stresses of thin-rimmed spur gears and with inclined webs. *Mech Mach Theory* 2013; 59: 34–47.
29. Guilbert B, Velex P, Dureisseix D, et al. Modular hybrid model to simulate the static and dynamic behavior of high-speed thin-rimmed gears. *J Sound Vib* 2019; 438: 353–380.
30. Herting DN. A general purpose, multi-stage component modal synthesis method. *Finite Elem Anal Des* 1985; 1: 153–164.
31. Guilbert B, Velex P, Dureisseix D, et al. A mortar based mesh interface for hybrid finite element/lumped parameter gear dynamic models – Application to thin-rimmed geared systems. *J Mech Des* 2016; 138: 1233301–1–11.
32. Bruyère J, Gu X and Velex P. On the analytical definition of profile modifications minimizing transmission error variation in narrow-faced spur helical gear. *Mech Mach Theory* 2015; 92: 257–272.